

## Nucleon Structure Functions from High Energy Neutrino Interactions with Iron and QCD Results

D.B. MacFarlane<sup>1</sup>, M.V. Purohit<sup>2</sup>, R.L. Messner<sup>3</sup>, D.B. Novikoff<sup>4</sup>

California Institute of Technology, Pasadena, CA 91125, USA

R.E. Blair, F.J. Sciulli, M.H. Shaevitz

Columbia University, New York, NY 10027, USA

H.E. Fisk, Y. Fukushima<sup>5</sup>, B.N. Jin<sup>6</sup>, Q.A. Kerns, T. Kondo<sup>5</sup>, P.A. Rapidis, S.L. Segler, R.J. Stefanski, D. Theriot, D.D. Yovanovitch

Fermilab, Batavia, IL 60510, USA

A. Bodek, R.N. Coleman<sup>2</sup>, W.L. Marsh<sup>2</sup>

University of Rochester, Rochester, NY 14627, USA

O.D. Fackler, K.A. Jenkins<sup>7</sup>

Rockefeller University, New York, NY 10021, USA

Received 5 March 1984

**Abstract.** Nucleon structure functions obtained from neutrino and anti-neutrino scattering on iron nuclei at high energies ( $E_\nu = 30$  to  $250$  GeV) are presented. These results are compared with the results of other lepton-nucleon scattering experiments. The structure functions are used to test the validity of the Gross-Llewellyn-Smith sum rule, which measures the number of valence quarks in the nucleons, and to obtain leading and second order QCD fits.

### 1. Experiment

We report results for the structure functions  $F_2(x, Q^2)$  and  $xF_3(x, Q^2)$  obtained from a high statis-

tics sample of neutrino and anti-neutrino charged current events. The data were taken using the Lab E detector in the dichromatic (narrow-band) neutrino beam at Fermilab. A total of 150,000 neutrino and 23,000 anti-neutrino charged current events were obtained in the experiment E616 at five momentum settings of the secondary beam: 120, 140, 168, 200 and 250 GeV/c.

Use of the dichromatic beam as the neutrino source allows a calculation of neutrino flux to be made from measured properties of the secondary hadron beam. This technique minimizes the overall systematic errors on both the total cross section [1] and structure function results. The dichromatic beam [2] consists of electrons, pions, kaons and protons produced by the interaction of 400 GeV/c primary protons with a BeO target; the particles are sign and momentum-selected by a point to parallel magnetic channel ( $\Delta p/p = 9.4\%$ ). The well collimated ( $\sigma_\theta = 0.2$  mr) secondary beam is then passed through an evacuated decay pipe where neutrinos are obtained from the weak decay of pions and kaons. A 910 m shield of earth and steel ranges-out the decay muons, leaving only neutrinos at Lab E.

The total flux of secondaries in the decay pipe was monitored using ionization chambers [3]. These

1 Now at the University of Toronto, Toronto, Ontario M5S1A7, Canada

2 Now at Fermilab, P.O. Box 500, Batavia, IL 60510, USA

3 Now at SLAC, Stanford, CA 94305, USA

4 Now at Hughes Aircraft Co., El Segundo, CA 90245, USA

5 Now at the National Laboratory for High Energy Physics, Tsukuba-gun, Ibaraki-ken 305, Japan

6 Now at the Institute for High Energy Physics, Peking, P.R. China

7 Now at the IBM Thomas J. Watson Research Center, P.O. Box 218, Yorktown Heights, NY 10598, USA

chambers have been calibrated using several different techniques. The estimated uncertainty in the absolute calibration is 2.5%. There is a further uncorrelated 1.6% and 4.2% error for neutrinos and anti-neutrinos respectively in applying the calibration measurement to conditions during data taking.

Secondary beam composition was determined using a Helium filled Cherenkov counter [3, 4]. The fraction of pions, kaons, and protons in the beam was determined by measuring the integrated Cherenkov light at a fixed angle to the beam as a function of counter pressure. The gas constant for the Cherenkov counter was measured using 200 GeV/c primary protons. Small corrections were made for backgrounds due to Cherenkov light from particles produced by interactions of the secondary beam with material upstream of the counter, and due to light scattering from dust on mirrors in the optical path. In addition, the analysis included the fact that a finite length radiator produces light within a diffractive envelope about the normal Cherenkov angle [4]. The counter response functions were predicted using a Monte Carlo calculation, and particle fractions were evaluated by fitting these functions to observed pressure curves. The estimated uncertainty in the determination of particle fractions is 1-4% for pions and 4-7% for kaons.

Beam direction and dispersion were measured using segmented ion chambers (SWICs). The mean direction of the secondary beam was maintained fixed to within a projected centroid of  $\pm 3.0$  cm at LabE, on a pulse by pulse basis. From the Cherenkov counter pressure curves mean momenta for kaons and protons were determined, a measurement redundant with the observed mean energy of neutrino events in the LabE apparatus. The consistency of these measurements indicates a systematic error in mean secondary momentum of less than 1.5%. Corrections to the neutrino flux were also made for neutrinos from decays before the momentum defining collimator (wide band background); this flux was measured by taking data with the collimator closed.

The LabE detector [5-7] (Fig. 1) consists of a calorimetric target of 640 t of 3 m square steel plates, interspersed with spark chambers (every 20 cm of steel) and liquid scintillation counters (every 10 cm of steel). This is followed by a steel toroidal spectrometer, 3.5 m in diameter, also instrumented with spark chambers (every 80 cm of steel) and scintillation counters (every 20 cm of steel). Measurements of hadronic energy and the outgoing muon angle are made in the target, and the muon momentum was determined by the spectrometer. The *rms* resolutions for these measurements are:

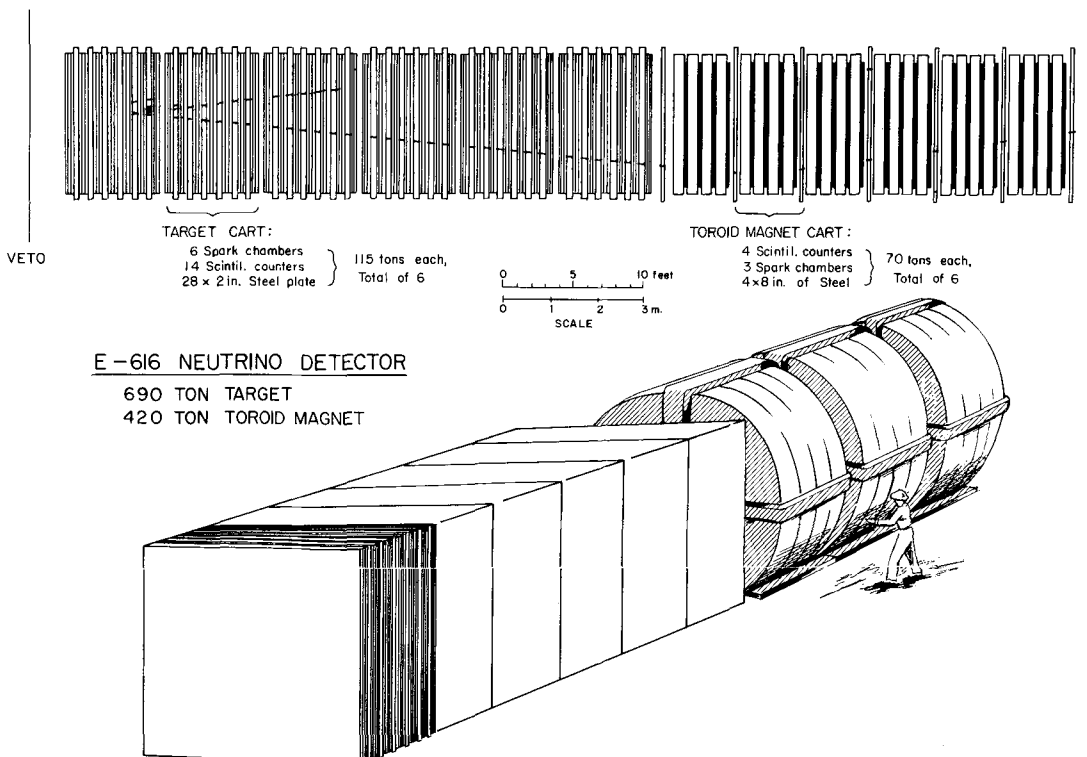


Fig. 1. The Lab E detector

$$\Delta E_H(\text{GeV}) = 0.93 + 0.78\sqrt{E_H}(\text{GeV})$$

$$\Delta E_\mu = 0.11 E_\mu$$

$$\Delta\theta_\mu(\text{mr}) = 106/E_\mu(\text{GeV})$$

where  $E_H$  and  $E_\mu$  are the final state hadron and muon energies respectively, and  $\theta_\mu$  is the outgoing muon angle.

## 2. Analysis

Two types of triggers were used to obtain data for the structure function measurement. The muon trigger required a secondary muon originating in the target region and penetrating through 1/3 of the spectrometer. No hadron energy requirement was made, but the acceptance of the spectrometer limited the kinematic coverage of the trigger to those muons with angle  $\theta_\mu < 250$  mr. The penetration trigger demanded a minimum hadron energy of 4 GeV in the target calorimeter, as well as a muon penetration of more than 160 cm in steel. Except for a common front veto counter requirement, the logic of the two triggers was independent. Both triggers are satisfied over a large kinematic region and the trigger efficiencies are determined to be  $99.5 \pm 0.5\%$  in the overlap region. Corrections of between 1% and 3% are made to compensate for the removal of events with poor fits to the muon track in the toroids.

Fiducial and kinematic cuts are applied to this data sample. Events due to neutrinos from pion decay are restricted to a region within a 76.2 cm radius of the beam center. Those events induced by kaon decay neutrinos are included within a 254 cm square, centered on the beam. Events are also confined to a longitudinal section of the target where hadron showers are fully contained within the target. Separation of events induced by neutrinos from pion and kaon decay, respectively, is extremely good [1].

Inclusive charged current events are usually parameterized by the quantities  $y = E_H/E_\nu$ ,  $Q^2 = 2E_\nu E_\mu(1 - \cos\theta_\mu)$  and  $x = Q^2/2ME_H$ . Kinematic cuts ensure good acceptance for events remaining after selection. These cuts are  $E_\mu > 4$  GeV and  $\theta_\mu < 200$  mr, well within the limits of acceptance for penetration and muon events respectively. A further cut on the hadron energy ( $E_H > 10$  GeV) eliminates part of the lower  $Q^2$  region where the  $x$  resolution is poor. The final data set after these cuts includes 65,000 neutrino and 7,000 anti-neutrino events.

The neutrino and anti-neutrino cross section in the standard ( $V - A$ ) theory can be written in terms of structure functions (apart from small correction terms):

$$\begin{aligned} \frac{d^2\sigma^{v(\bar{v})}}{dx dy} = & \frac{G^2 ME}{\pi} \\ & \cdot \left\{ \left( 1 - y - \frac{Mxy}{2E} + \frac{y^2}{2} \frac{1 + 4M^2 x^2/Q^2}{1 + R(x, Q^2)} \right) F_2(x, Q^2) \right. \\ & \left. \pm \left( y - \frac{y^2}{2} \right) xF_3(x, Q^2) \right\}. \end{aligned} \quad (1)$$

For an isoscalar target:

$$2xF_1(x, Q^2) = q(x, Q^2) + \bar{q}(x, Q^2)$$

$$F_2(x, Q^2) = 2xF_1(x, Q^2)(1 + R(x, Q^2))/(1 + 4M^2 x^2/Q^2)$$

$$xF_3(x, Q^2) = q(x, Q^2) - \bar{q}(x, Q^2) \quad (2)$$

where  $q = u + d + s + c$  and  $\bar{q} = \bar{u} + \bar{d} + \bar{s} + \bar{c}$  are respectively the quark and anti-quark momentum densities within the nucleon and  $R \equiv \sigma_L/\sigma_T$  is the ratio of cross-sections of longitudinally and transversely polarized vector bosons. In another notation, the structure functions described above are the average of neutrino and anti-neutrino structure functions of the nucleon. No measurement of  $R$  is reported here; the structure functions are extracted under various assumptions about  $R$  which are consistent with present experimental measurements [8]. The propagator term for charged currents, with boson mass  $M_W = 80$  GeV, is not shown in (1), but is included in all of the analysis described here.

From the form of the differential cross-section (1) it can be seen that the number of neutrino or anti-neutrino events in a given  $x$  and  $\log Q^2$  bin is a linear combination of  $F_2$  and  $xF_3$ :

$$\eta_\nu/c_\nu = a_\nu F_2(x, Q^2) + b_\nu xF_3(x, Q^2)$$

$$\eta_{\bar{\nu}}/c_{\bar{\nu}} = a_{\bar{\nu}} F_2(x, Q^2) + b_{\bar{\nu}} xF_3(x, Q^2). \quad (3)$$

The coefficients  $a_{v(\bar{v})}$  and  $b_{v(\bar{v})}$  are numerically evaluated integrals of products of flux and  $y$ -distribution factors. Various corrections need to be applied and are contained in  $c_{v(\bar{v})}$ . These include: (1) correction for the slightly non-isoscalar iron and scintillator target with a 6.5% excess of neutrons over protons, (2) strange sea correction, since the strange and charm components of the nucleon are not equal, (3) radiative corrections, following the prescription of de Rújula et al. [9] and (4) bin center corrections. For the strange sea correction it was assumed that the charm component was zero and that the strange component of the sea (1/2  $SU(3)$  symmetric) [10, 11]. The sea was obtained from fits to our structure function results. The suppression of transitions of  $d$  and  $s$  quarks to  $c$  was accounted for using slow-rescaling [21] with a charm quark mass of 1.5 Ge-

$V/c^2$ . Corrections for acceptance are made by either weighting each event, or by including acceptance in the calculation of  $a_{\nu(\bar{\nu})}$  and  $b_{\nu(\bar{\nu})}$ . Both approaches have been used with consistent results. Weights and acceptance are calculated in a model independent fashion by taking advantage of the symmetry of the cross-section (1) with respect to rotations about the beam axis. Finally, the effect of resolution smearing is removed by correcting the observed number of events,  $n_{\nu(\bar{\nu})}$ , by a Monte Carlo determined correction factor.

Total cross-sections from this experiment have been reported earlier and average about 10% higher [1] than some previous results. Therefore, the integrals of structure functions at fixed  $E_\nu$  or  $Q^2$  are also

higher. Assuming simple scaling, it is possible to obtain the integrals of  $F_2$  and  $xF_3$  from the  $\nu$  and  $\bar{\nu}$  cross-section slopes determined by various experiments. The actual integrals may differ from these values due to experimentally observed levels of scale breaking which should be less than  $\sim 3\%$ . Table 1 is a comparison of integrals obtained from the cross sections and those we obtained by integrating the structure functions reported by the same experiments. Our results are quoted for two values of  $R$  to facilitate the comparisons. The integrals from the two techniques are in good agreement except for those from CDHS and the integral of  $F_2$  from HPWF. The table implies then that the difference in integrals of structure functions reported by us and

**Table 1.** Integrals of structure functions compared with the same integrals obtained from cross-sections. In all cases the assumptions are made about the strange sea ( $1/2 SU(3)$  symmetric), slow rescaling and the  $W$ -boson propagator. Some of the structure functions are extrapolated to cover the entire  $x$ -region. All these effects, along with scale breaking, do not change the results above by more than  $\sim 3\%$ . All cross-section slopes are in units of  $10^{-38} \text{ cm}^2/\text{GeV}$

	CCFRR	CCFRR	CDHS	CHARM	HPWF
Reference	[1], This expt.	[1], This expt.	[11, 12]	[13, 14]	[15]
$\sigma_\nu/E$	$0.669 \pm 0.024$	$0.669 \pm 0.024$	$0.62 \pm 0.022$	$0.604 \pm 0.032$	$0.63 \pm 0.02$
$\sigma_{\bar{\nu}}/E$	$0.340 \pm 0.020$	$0.340 \pm 0.020$	$0.30 \pm 0.013$	$0.301 \pm 0.018$	$0.30 \pm 0.01$
$R$	0.0	0.1	0.1	0.0	0.0
$\int F_2$ predicted from cross-sections	$0.466 \pm 0.015$	$0.478 \pm 0.015$	$0.436 \pm 0.012$	$0.418 \pm 0.017$	$0.430 \pm 0.010$
$\int xF_3$ predicted from cross-sections	$0.312 \pm 0.030$	$0.312 \pm 0.030$	$0.303 \pm 0.024$	$0.287 \pm 0.035$	$0.313 \pm 0.021$
$\int F_2$ from structure function results (statistical errors only)	$0.474 \pm 0.003$	$0.482 \pm 0.003$	$0.402 \pm 0.002$	$0.412 \pm 0.006$	$0.458 \pm 0.003$
$\int xF_3$ from structure function results (statistical errors only)	$0.328 \pm 0.005$	$0.326 \pm 0.005$	$0.273 \pm 0.003$	$0.285 \pm 0.012$	$0.322 \pm 0.005$

**Table 2.** Total cross-section slopes in energy bins with and without the flux smoothing procedure. To avoid repetition, errors are only shown on one set and are statistical first and systematic second (they do not include an overall scale error of 3% for neutrinos and 5.5% for anti-neutrinos). All cross-section slopes are in units of  $10^{-38} \text{ cm}^2/\text{GeV}$

$E_\nu$ (GeV)	$\sigma_\nu/E$ Before corr.	$\sigma_\nu/E$ After corr.	$E_{\bar{\nu}}$ (GeV)	$\sigma_{\bar{\nu}}/E$ Before corr.	$\sigma_{\bar{\nu}}/E$ After corr.
37.1	$0.654 \pm 0.012 \pm 0.019$	0.691	36.9	$0.361 \pm 0.010 \pm 0.015$	0.340
44.7	$0.621 \pm 0.010 \pm 0.020$	0.664	45.0	$0.352 \pm 0.007 \pm 0.013$	0.331
54.0	$0.661 \pm 0.008 \pm 0.018$	0.696	54.0	$0.350 \pm 0.007 \pm 0.013$	0.342
63.5	$0.664 \pm 0.010 \pm 0.024$	0.695	63.8	$0.332 \pm 0.009 \pm 0.014$	0.344
75.4	$0.664 \pm 0.008 \pm 0.028$	0.686	75.6	$0.331 \pm 0.009 \pm 0.020$	0.342
91.0	$0.644 \pm 0.015 \pm 0.057$	0.668	89.3	$0.333 \pm 0.015 \pm 0.031$	0.346
111.7	$0.659 \pm 0.029 \pm 0.058$	0.664	110.3	$0.314 \pm 0.022 \pm 0.034$	0.324
124.8	$0.665 \pm 0.020 \pm 0.037$	0.661	126.5	$0.341 \pm 0.017 \pm 0.032$	0.318
141.2	$0.695 \pm 0.026 \pm 0.043$	0.688	150.0	$0.339 \pm 0.015 \pm 0.022$	0.351
157.4	$0.680 \pm 0.018 \pm 0.033$	0.668	174.4	$0.321 \pm 0.015 \pm 0.021$	0.354
165.1	$0.714 \pm 0.020 \pm 0.035$	0.666	201.9	$0.303 \pm 0.017 \pm 0.026$	0.340
179.8	$0.727 \pm 0.015 \pm 0.036$	0.680			
190.8	$0.749 \pm 0.015 \pm 0.035$	0.694			
212.5	$0.709 \pm 0.014 \pm 0.048$	0.637			
229.1	$0.756 \pm 0.018 \pm 0.052$	0.680			
Average	$0.669 \pm 0.003 \pm 0.024$			$0.340 \pm 0.003 \pm 0.020$	

CDHS is only partly explained by total cross-section differences.

$F_2$  and  $xF_3$  are extracted with the constraint that the integrals of structure functions in overlapping  $x$  and  $Q^2$  regions at different energy settings of the secondary beam be the same. This procedure removes most of the uncertainty induced by the errors on particle fractions in the decay pipe. The required adjustments to the  $\nu$  and  $\bar{\nu}$  fluxes are consistent with the expected errors on particle fractions from the Cherenkov analysis and are in excellent agreement with a cross-section rising linearly with energy. Table 2 lists our measurements of the total cross-section slopes before and after this procedure.

The structure functions resulting from our analysis are shown in Table 7 for the assumptions  $R=0.1$  and  $R_{\text{QCD}}$  (see (11)). The errors shown in the table are statistical only. Figures 8 and 9 show the results assuming  $R=R_{\text{QCD}}$ .

### 3. Quark-Parton Model Tests

These results have been compared with predictions of the Quark-Parton model and of QCD [25, 26]. The Quark-Parton model relates  $F_2^{\mu N}$  obtained from charged lepton scattering to that obtained from neutrino scattering by the mean square charge of the constituent quarks:

$$F_2^{\text{PRED}} = \frac{18}{5} F_2^{\mu N} \left/ \left( 1 - \frac{3}{5} \frac{s + \bar{s}}{q + \bar{q}} \right) \right. \quad (4)$$

taking  $c = \bar{c} = 0$ . Comparisons of structure functions from various neutrino and muon scattering experiments can therefore be made. For these comparisons it was again assumed that the strange sea is  $1/2$   $SU(3)$  symmetric. The ratio of  $F_2$  from this data to  $F_2^{\text{PRED}}$ , as calculated from published muon scattering data from iron by the European Muon Collaboration (EMC) [16] is shown in Fig. 2. Both data sets have been interpolated to  $Q^2 = 10 \text{ GeV}^2/c^2$  in this comparison, and the value of  $F_2^{\mu N}$  adjusted to the assumption of  $R=0.1$ . The predicted value falls below our measurement by about 10%, but exhibits no  $x$  dependence. This is near the combined estimated systematic normalization errors of 3% for EMC and 5% for our result. There has been some evidence that the normalization of the result from EMC is systematically lower than that of other charged lepton scattering experiments [17]. A recent measurement [18] of  $F_2^{\mu N}$  from iron is also systematically larger than EMC values by 4.7%. The comparison between neutrino and muon data is not seriously affected by assumptions about the strange

sea, either in evaluating  $F_2^{\text{PRED}}$  or in extracting  $F_2$  from neutrino scattering data. Reasonable changes in assumptions about the strange sea or the charm quark mass do not appreciably change the result. Also included in Fig. 2 is the corresponding result using  $F_2$  from CDHS [12] modified to include the effects of a massive charmed quark with  $m_c = 1.5 \text{ GeV}/c^2$ . The difference between results obtained for  $F_2$  reported here and CDHS is not simply a level difference as implied by the difference in the total cross sections. Our result for  $F_2$  is more strongly peaked at small  $x$  than the data of CDHS. We have considered the possibility that the differences between our data and those of CDHS arise because of errors in the various corrections applied. These include bin-centre, strange sea, isoscalar, charm mass, radiative and smearing corrections. All corrections are of the order of 5–10% and often less; we estimate that the errors in reported structure function data points due to uncertainties in these corrections are always less than 2–3%.

Also sensitive to overall levels is the test of the Gross-Llewellyn-Smith (GLS) sum rule:

$$\int_0^1 F_3(x, Q^2) dx = 3 \left( 1 - \frac{\alpha_s(Q^2)}{\pi} \right). \quad (5)$$

Equation (5) is the prediction including the  $O(\alpha_s)$  correction from QCD beyond the leading log approximation. The experimental result for the GLS sum rule [26] is strongly influenced by the determination of  $xF_3$  at low  $x$ . Roughly half of the integral over  $F_3$  comes from the region below  $x=0.06$ . The

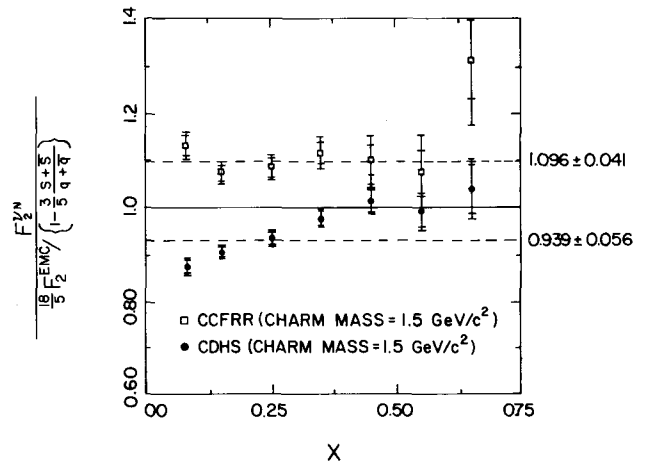


Fig. 2. Ratio of  $F_2$  for CCFRR and CDHS to  $F_2^{\text{PRED}}$  from EMC at  $Q^2 = 10 \text{ GeV}^2$ . The numbers on the right are averages which include overall normalization errors. The CDHS data have been adjusted for the effects of a massive charmed quark assuming that  $m_c = 1.5 \text{ GeV}/c^2$

excellent small  $x$  resolution of this experiment allows us to make a nearly model independent measurement. Since the small  $x$  region is critical, a result can only be obtained at low  $Q^2$ . Because the values of  $E_h$  are high, these data are typically at high  $W^2$ . At  $Q^2 = 3 \text{ GeV}^2$ , we obtain

$$\int_0^1 F_3(x) dx = 2.83 \pm 0.15 \pm 0.09 \pm 0.10$$

where the first error is statistical, the second comes from correlated  $\nu$  and  $\bar{\nu}$  flux errors and the third accounts for other systematic errors. Fine bins were made at low  $x$  and in every bin the data been interpolated to a fixed  $Q^2$ . The integral of  $F_3$  above  $x=0.01$  is virtually independent of the integration technique used, including direct summation of  $x F_3/x$ . The error for the  $x < 0.01$  region is dominated by the error in the exponent of  $x$  in fits of the form  $Ax^{b_3}$ . A fit using the region  $x < 0.06$  gives  $b_3 = 0.58 \pm 0.18$ , whereas a global fit ( $0 < x < 1$ ) using the form in (8) gives  $b_3 = 0.58 \pm 0.06$ . The expectation [19] that  $x F_3$  behaves like  $\sqrt{x}$  at small  $x$  is also satisfied. The global QCD fit in Sect. 4 gives  $2.70 \pm 0.15$  for the value of  $\int_0^1 F_3 dx$  at  $Q_0^2 = 12.6 \text{ GeV}^2$ . All of these values are consistent with QCD expectations for  $\Lambda_{\text{LO}} < 525 \text{ MeV}$  using statistical errors. Figure 3 shows the variation in  $x F_3$  as a function of  $x$  (on a log scale). The integrated value of  $F_3$  is also shown. The consistency with  $\sqrt{x}$  at small values of  $x$  is obvious.

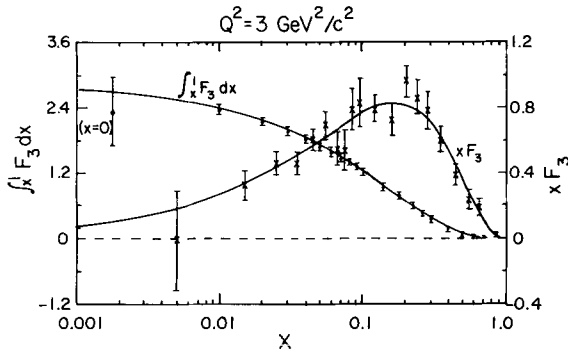


Fig. 3.  $x F_3$  in fine  $x$  bins at  $Q^2 = 3 \text{ GeV}^2$  with the fit (8). Also shown is  $\int_0^1 F_3 dx$  from the fit with points from the simple summation technique superimposed. The right scale (crosses) is  $x F_3$  at  $Q^2 = 3 \text{ GeV}^2$ . The left scale (diamonds) corresponds to  $\int_0^1 F_3 dx$  at  $Q^2 = 3 \text{ GeV}^2$ . In the most important region  $x < 0.06$ ,  $W^2$  is always larger than  $16.5 \text{ GeV}^2$

#### 4. QCD Formalism

QCD predicts logarithmic scaling violations in the structure functions due to quark bremsstrahlung and gluon pair production processes which increase with decreasing distance over which the nucleon is probed. This effect is described by the Altarelli-Parisi equations [20] which allow the calculation of the values of the structure functions at some evolved  $Q^2$ , given the structure function at some  $Q_0^2$ . In leading order:

$$\begin{aligned} \frac{dF_2(x, Q^2)}{d \ln Q^2} &= \frac{\alpha_s(Q^2)}{2\pi} \{P_{qq}(x) \otimes F_2(x, Q^2) + 2N_f P_{gq}(x) \otimes G(x, Q^2)\} \\ \frac{dG(x, Q^2)}{d \ln Q^2} &= \frac{\alpha_s(Q^2)}{2\pi} \{P_{qg}(x) \otimes F_2(x, Q^2) + P_{gg}(x) \otimes G(x, Q^2)\} \\ \frac{dx F_3(x, Q^2)}{d \ln Q^2} &= \frac{\alpha_s(Q^2)}{2\pi} \{P_{qq}(x) \otimes x F_3(x, Q^2)\} \end{aligned} \quad (6)$$

where the terms in brackets are of the general form:

$$f(x) \otimes g(x) = \int_x^1 f(z) g\left(\frac{x}{z}\right) \frac{dz}{z}$$

The  $P_{ij}$  are splitting functions given by QCD, and  $G(x, Q^2)$  is the gluon distribution of the nucleon. The strong coupling constant is, to leading order,

$$\alpha_s(Q^2) = \frac{12\pi}{(33 - 2N_f) \ln Q^2 / \Lambda_{\text{LO}}^2} \quad (7)$$

where the scale parameter  $\Lambda_{\text{LO}}$  is to be experimentally determined. The number of quark flavors,  $N_f$ , was taken to be four.

The procedure used to determine  $\Lambda$  is to parameterize  $F_2$ ,  $G$  and  $x F_3$  at some  $Q_0^2$ :

$$\begin{aligned} F_2(x, Q_0^2) &= a_2 (1-x)^{e_2} (1 + \gamma_2 x) \\ x F_3(x, Q_0^2) &= a_3 x^{b_3} (1-x)^{e_3} \\ G(x, Q_0^2) &= a_G (1-x)^{e_G} (1 + \gamma_G x) \end{aligned} \quad (8)$$

and then to use the evolution equations to compute the predicted value at any other  $Q^2$ . Separate least square fits to  $F_2$  and  $x F_3$  are used to extract the various unknown parameters and  $\Lambda$ . Target mass corrections are very small in the regions of  $x$  and  $Q^2$  studied and are applied using the prescription of Georgi and Politzer [21] for the  $F_2$  analysis. For the

purposes of the  $xF_3$  analysis we have verified that these corrections are small ( $<3\%$  change in  $\alpha_s$ ) in the regions studied.

## 5. $F_2$ Analysis

The structure function  $F_2$  is proportional to the sum of neutrino and anti-neutrino differential cross sections, and therefore has small fractional statistical errors. However the  $Q^2$  evolution of  $F_2$  is complicated by the coupling to the unknown gluon distribution  $G$ . In addition, extraction of this structure function is sensitive to assumptions about  $R$  and the strange sea. Fits are made to the data in the region  $Q^2 > 5 \text{ GeV}^2$  and  $W^2 > 10 \text{ GeV}^2$  where corrections from the finite target mass, higher twist and quark mass thresholds are small. We use a computer program obtained from Duke and Owens and described in [23] for both first and second order fits. Data below  $x=0.1$  are eliminated to limit reliance on uncertain assumptions about the strange sea. The normalization of the gluon distribution at  $Q_0^2 = 5 \text{ GeV}^2$  is constrained by the momentum sum rule:

$$\int_0^1 G(x, Q^2) dx = 1 - \int_0^1 F_2(x, Q^2) dx. \quad (9)$$

A QCD fit using the  $F_2$  values from this experiment (Table 7) with fixed reasonable gluon parameters ( $c_G = 4.6$  and  $\gamma_G = 9.0$ ), yielded the parameters listed in Table 3. The second order fit, made using the method of [23], is shown in the last column of the table. The fit is slightly worse than the leading order fit and the value of  $A$  is slightly larger.

In leading order QCD,  $R$  is expected to be zero. We denote this contribution to  $R$  by  $R_{\text{QCD}}$ . To second order, the longitudinal structure function  $F_L (= 2xF_1R)$  is given by

$$F_L = \frac{\alpha_s(Q^2)}{2\pi} x^2 \int_x^1 \frac{dy}{y^3} \cdot \left\{ \frac{8}{3} F_2(y, Q^2) + 4n_f \left(1 - \frac{x}{y}\right) yG(y, Q^2) \right\}. \quad (10)$$

This implies that  $R$  is small at large  $x$ , large at small  $x$  and decreases logarithmically with increasing  $Q^2$ . Using a modified version of our  $F_2$  evolution program we have parameterized the dependence of  $R$  on  $F_2$  and  $G$  by the form

$$R = \frac{0.73(1-x)^{3.7}}{\ln(Q^2/0.24^2)}. \quad (11)$$

Values for  $A$  have been extracted using  $R_{\text{QCD}}$  and the assumptions  $R=0$  and  $R=0.1$ . They are also listed in Table 3 and all lie within 160 MeV of each other.

It is well known [22, 23] that the fitted value of  $A$  is strongly correlated with the parameters characterizing the gluon distribution. Fits using  $F_2$  alone are unable to significantly constrain these gluon parameters. The Quark-Parton model and asymptotic QCD [24] predict that the gluon distribution behaves at large  $x$  like  $(1-x)^{c_3+1}$ . As reported below fits to  $xF_3$  show that  $c_3 \approx 3.4$ . It is reasonable to expect that the gluon parameters lie within the limits:  $4 \leq c_G \leq 8$  and  $\gamma_G \geq 0$ . The correlation between the best value for  $A_{\text{LO}}$  and  $c_G$  for various values of  $\gamma_G$  is shown in Fig. 4. The rms contribution to the determination of  $A$  is found to be about  $\pm 50 \text{ MeV}$ ,

**Table 3.**  $F_2$  fits with  $c_G = 4.6$ ,  $\gamma_G = 9.0$  and  $R = 0.1$

	Leading order	Second order ( $\overline{\text{MS}}$ )
$A$	$360 \pm 100 \text{ MeV}$	$340 \pm 110 \text{ MeV}$
$c_2$	$2.85 \pm 0.16$	$3.36 \pm 0.15$
$a_2$	$1.525 \pm 0.086$	$1.808 \pm 0.092$
$\gamma_2$	$1.87 \pm 0.56$	$2.14 \pm 0.57$
$\chi^2$	45.5 for 39 DF	45.5 for 39 DF
	$A_{\text{LO}}$	$A_{\overline{\text{MS}}}$
$R=0.0$	$360 \pm 100 \text{ MeV}$	$390 \pm 110 \text{ MeV}$
$R=0.1$	$200 \pm 90 \text{ MeV}$	$230 \pm 100 \text{ MeV}$
$R_{\text{QCD}}$	$300 \pm 100 \text{ MeV}$	$340 \pm 110 \text{ MeV}$

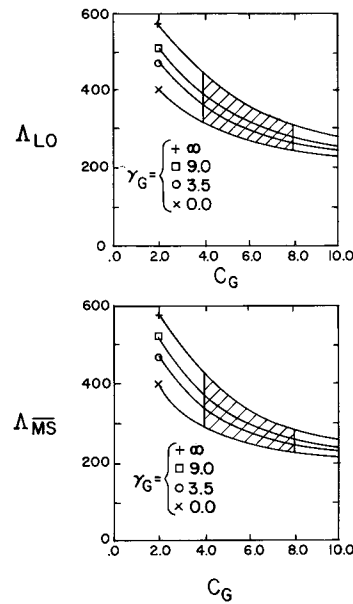


**Fig. 4.** Correlation between best values for  $A$  from  $F_2$  and gluon parameters

**Table 4.** Estimated systematic errors on  $A_{LO}$  from fits to  $F_2$ 

Source	Change in $A_{LO}$
Gluon distribution	$\pm 50$ MeV
Strange sea	$\pm 35$ MeV
Flux smoothing	$\pm 25$ MeV
Flux level	$\pm 30$ MeV
Secondary beam dispersion	$\pm 10$ MeV
Hadron energy calibration	$\pm 15$ MeV
Muon energy calibration	$\pm 15$ MeV
Total, excluding gluon dist.	$\pm 57$ MeV

if all values of the gluon parameters within the noted limits are equally probable.

Table 4 shows changes in  $A_{LO}$  for variation of several assumptions made in fitting  $F_2$ . The single largest source of uncertainty in  $A_{LO}$  arise from assumptions about the gluon distribution. The strange sea uncertainty contributes the next largest error. The errors due to uncertainties in the setting to setting  $\nu$  and  $\bar{\nu}$  fluxes from our smoothing technique and those from overall level uncertainties are also shown.

## 6. $xF_3$ Analysis

The structure function  $xF_3$  measured in deep inelastic neutrino scattering is unique in that the extracted value of this structure function is almost independent of the value of  $R$ , and its QCD evolution does not depend on the gluon density. However, since  $xF_3$  is essentially the difference of the  $\nu$  and  $\bar{\nu}$  differential cross-sections, it has larger fractional statistical errors than  $F_2$ .

Two different computer programs have been used to evolve  $xF_3$  to both first and second order [20]: one was obtained from Barnett [22] and the previously mentioned one from Duke and Owens [23]. The programs solve the differential equation (6) to first and second order starting at  $Q_0^2$  ( $12.6 \text{ GeV}^2$ ) with the parameterization of  $xF_3(x, Q_0^2)$  shown in (8). The GLS sum rule (5) is not used to constrain the normalization since the very small  $x$  region is not being used in these fits. The constants  $a_3$ ,  $b_3$  and  $c_3$  are determined as parameters along with  $A$ . Cuts are imposed to eliminate regions where non-perturbative QCD effects may be significant. These are:

$$Q^2 > 5 \text{ GeV}^2, \quad W^2 > 10 \text{ GeV}^2, \quad 0.04 < x < 0.7.$$

It should be noted that the two programs agree well in leading order. At the 90% CL we find that  $A_{LO} < 420$  MeV. The best fit parameters are

$$A_{LO} = 88^{+163}_{-78} \text{ MeV}$$

$$\alpha_S = 0.204 \pm 0.079 \quad \text{for } Q_0^2 = 12.6 \text{ GeV}^2$$

$$b_3 = 0.672 \pm 0.058$$

$$c_3 = 3.29 \pm 0.24$$

$$a_3 = 4.34 \pm 0.24$$

$$\chi^2 = 44.2 \quad \text{for 45 DF.} \quad (12)$$

The curve labelled “ $xF_3$ ” in Fig. 5 shows the  $\chi^2$  versus  $A$  for this fit. Note that, this best value for  $A_{LO}$  from  $xF_3$ , together with the results from  $F_2$  shown in Fig. 4, indicate that larger values of  $c_G$  i.e., “softer” gluon distributions, are preferred. This is a weak conclusion at present, because of the limited statistical precision of the data.

The same non-singlet analysis has been performed by the standard technique [23] of combining experimental values of  $xF_3$  below  $x=0.4$  and  $F_2$  above  $x=0.4$ . This implicitly assumes a vanishing sea and small  $R$  in the high- $x$  region, or equivalently that  $xF_3 = F_2$  above  $x=0.4$ . The resulting parameters agree with those above:

$$A_{LO} = 266^{+114}_{-104} \text{ MeV}$$

$$\alpha_S = 0.291 \pm 0.047 \quad \text{for } Q_0^2 = 12.6 \text{ GeV}^2$$

$$b_3 = 0.635 \pm 0.049$$

$$c_3 = 2.90 \pm 0.13$$

$$a_3 = 4.29 \pm 0.22$$

$$\chi^2 = 50.0 \quad \text{for 46 DF.}$$

The curve labelled “ $xF_3/F_2$ ” in Fig. 5 shows the  $\chi^2$  versus  $A$  for this fit. The substantial reduction in errors is quite clear in the figure.

The non-linear nature of the dependence of the evolution equations (6) on  $A$ , combined with large statistical errors on  $xF_3$ , results in the asymmetric shape of the curves in Fig. 5. The dependence of  $\chi^2$  on  $\alpha_S(Q_0^2 = 12.6 \text{ GeV}^2)$  is shown in Fig. 6. Because of the more linear dependence on  $\alpha_S$  in (6), these curves are much more symmetric. For this reason, in the investigation of changes due to several systematic effects below, we look at the behaviour of  $\alpha_S(Q_0^2 = 12.6 \text{ GeV}^2)$  instead of the behaviour of  $A$ . It should be noted that from either fit, the hypothesis that  $\alpha_S = 0$  or  $A = 0$  is poor ( $\chi^2 = 52.7$ , 46 d.f. for  $xF_3$  alone;  $\chi^2 = 100.6$ , 47 d.f. for “ $xF_3/F_2$ ”). In both cases, the  $\chi^2$  at the best fit is acceptable using statistical errors only.

Possible correlations among the parameters were

determined from the fit to  $xF_3$  alone,  $\alpha_s(Q_0^2)$  has virtually no correlation with  $\int F_3 dx$  and with  $b_3$ . The correlation with  $c_3$  however, is strong, and is shown in Fig. 7. This indicates that the high- $x$  dependence of  $xF_3$  affects the value of  $A$  to some extent.

The parameters in (12) imply  $\int F_3 dx = 2.70 \pm 0.15$  as quoted in Sect. 4. This value is consistent with the result of the GLS sum rule analysis. It should be noted that this fit does not utilize the very low- $x$  data. The reduced statistical error is related to the additional constraints imposed by the specific parameterization, (8).

The effects of changing the forms of the fitting functions were not found significant; for example, increasing the number of parameters in the fit by the inclusion of a  $(1 + \gamma x)$  term does not change  $A$  significantly.  $A$  is also unaffected by varying the  $Q_0^2$  at which  $xF_3$  is parameterized and by iterating the structure function extraction. Columns 2 and 3 of Table 5 show the changes in  $\alpha_s(Q_0^2)$  resulting from these and several other changes in the assumptions made in extracting structure function values and using them in the two fits described above. The last four items give the effect of changing the number of flavors, including the  $(1 + \gamma x)$  term, changing  $Q_0^2$  and changing assumptions about the strange sea. These have very little effect on  $\alpha_s(Q_0^2)$ .

The first two items in the table, which produce larger changes in  $\alpha_s$ , require some comment. As mentioned previously, the data used here were obtained at several different beam energy settings. The resulting cross-section slopes are consistent, within expected fluctuations, with being independent of energy as well as with the small dependence on energy calculated from integrating the QCD parameterization. Since any quark-parton model would give a smooth dependence on energy, the data were constrained to satisfy this hypothesis. This was done by requiring that the number of events at a given energy setting agree with a prediction from integrals of the averaged structure functions. The changes in  $\alpha_s$  tabulated in the first row result from the variations within the errors of our cross-section smoothing procedures. The value of  $xF_3$ , since it comes from the difference in neutrino and anti-neutrino data, is sensitive to the uncorrelated normalization errors in the cross-section measurements. The numbers in the second row reflect the changes in  $\alpha_s(Q_0^2)$  calculated due to these errors. Although these effects are smaller than the statistical error on  $\alpha_s$ , it is clear that precise measurements of  $A$  with this technique require high precision on normalized cross-sections.

The sensitivity of the alternative method, which used  $F_2$  values at large  $x$ , is also shown in Table 5.

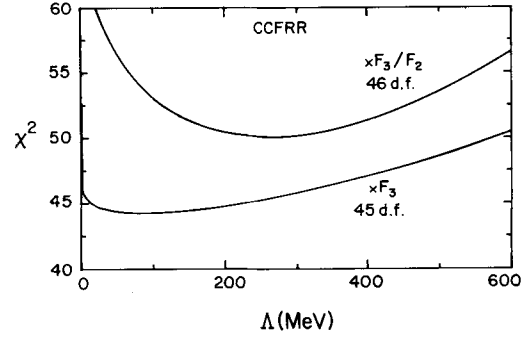


Fig. 5.  $\chi^2$  versus  $\Lambda_{LO}$  for fits to  $xF_3$  and " $xF_3/F_2$ "

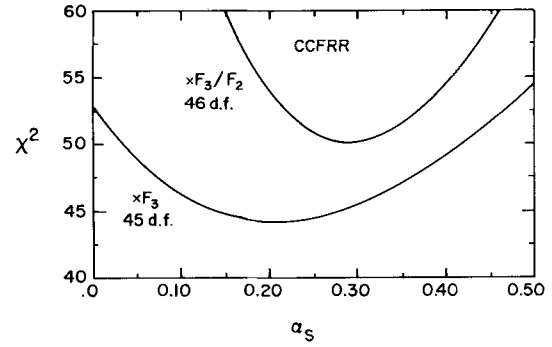


Fig. 6.  $\chi^2$  versus  $\alpha_s$  for fits to  $xF_3$  and " $xF_3/F_2$ "

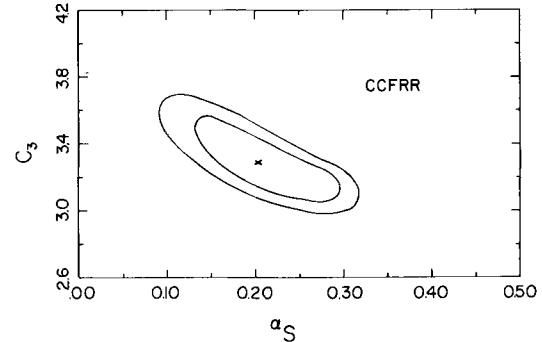


Fig. 7. Correlation between  $\alpha_s$  and  $c_3$  used in fitting  $xF_3$ . Shown are one and two standard deviation contours

The different sensitivity with this method reflects both the different way  $F_2$  depends on the assumptions and the different statistical precision of this data. In all cases, these changes in  $\alpha_s$  (or  $A$ ) are smaller than the statistical errors of 0.079 for the  $xF_3$  fit and 0.047 for the " $xF_3/F_2$ " fit. It should be noted that the first two systematic errors which come from flux uncertainties, while valid for this

**Table 5.** Estimated effect on  $\alpha_S$  due to changes in assumptions

Systematic effect	$xF_3$	" $xF_3/F_2$ "
Cross-section smoothing	0.027	0.010
Cross-section level errors	0.047	0.006
$n_f=4$ changed to $n_f=3$	0.001	0.003
Inclusion of $\gamma_x$ term	0.0003	0.002
Change in $Q_0^2(12.6 \text{ GeV}^2)$	0.001	0.001
1/2 $SU(3)$ changed to $SU(3)$	0.002	0.002
Different $R$ assumptions	0.004	0.015
Different models for correction terms in $F_2, xF_3$ extraction	0.008	0.006
Systematic error in $E_{\text{HAD}}$	0.011	0.011
Systematic error in $E_\mu$	0.014	0.009
Beam angular dispersion error	0.019	0.024

**Table 6.**  $\Lambda$  and  $\alpha_S$  resulting from first and second ( $\overline{\text{MS}}$ ) order fits

Method	$\Lambda$ (MeV)	$\alpha_S(Q^2 = 12.6 \text{ GeV}^2)$
Leading Order	88 <sup>+163</sup> - 78	$0.204 \pm 0.079$
$\overline{\text{MS}}$ Barnett [22]	120 <sup>+200</sup> -106	$0.176 \pm 0.062$
$\overline{\text{MS}}$ Duke [23]	193 <sup>+272</sup> -156	$0.201 \pm 0.070$

experiment, are partially limited by statistics and should be smaller for a higher statistics experiment.

Finally, we remark on several attempts to fit the data using prescriptions for second-order QCD. These should each give  $\Lambda_{\overline{\text{MS}}}$ , the scale parameter in the modified minimal subtraction scheme, which should minimize the differences from  $\Lambda_{\text{LO}}$ . In contrast to the agreement among the leading-order fits, we find some differences between the second order fits using the two available computer programs [22, 23]. Table 6 shows the values of  $\Lambda$  and  $\alpha_S$ , with statistical errors, resulting from these fits.

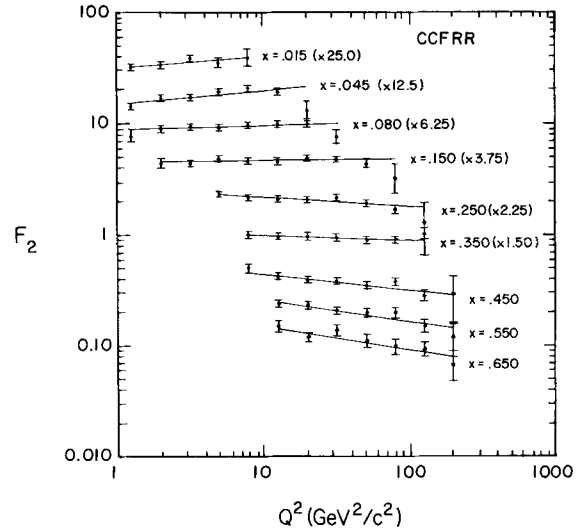
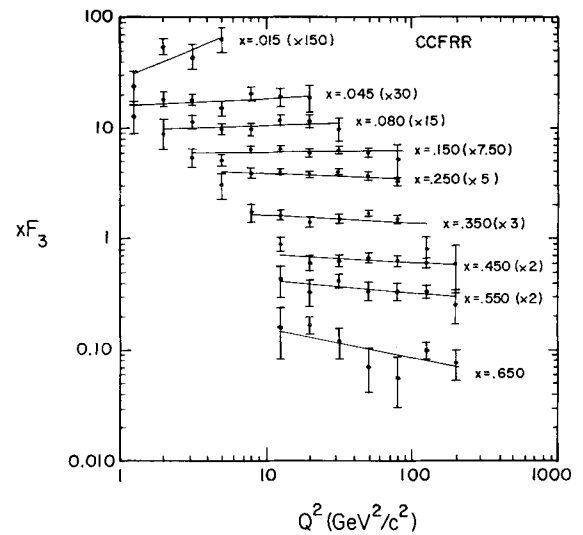
There are technical differences among the programs. That of Duke and Owens [23] uses a definition of parton densities that makes them "universal", the same densities applicable in any process. Structure functions are constructed from evolved parton densities. The other technique [22] is one in which certain cross section terms are absorbed into the definition of parton densities and the structure functions are evolved directly [24]. In principle, both programs should give the same value for  $\Lambda_{\overline{\text{MS}}}$  if the true expression (or functional form) for  $xF_3$  and the parton density were known at  $Q^2 = Q_0^2$  and if all non-perturbative effects were absent. However, since these expressions are unknown, both the computer programs utilize the *same* parameterization for these

*different* distributions and therefore lead to the different values for  $\Lambda_{\overline{\text{MS}}}$ . It should be noted that the change in  $\alpha_S(Q_0^2)$  in going from leading to second order is not large.

## 7. Conclusions

The high statistics neutrino-nucleon scattering data from the Fermilab experiment E616 have been used to extract the  $F_2$  and  $F_3$  structure function data shown in Table 7. From this data, it is concluded:

(1) The Quark-Parton model comparison of  $F_2(x)$  with the analogous structure function mea-

**Fig. 8.**  $F_2(x, Q^2)$  assuming  $R = R_{\text{QCD}}$  (see text)**Fig. 9.**  $xF_3(x, Q^2)$  assuming  $R = R_{\text{QCD}}$  (see text)

**Table 7.**  $F_2(x, Q^2)$  and  $xF_3(x, Q^2)$  for  $R_{\text{QCD}}$  and  $R=0.1$  (statistical errors only)

$x$	$Q^2$	$F_2$ ( $R=0.1$ )	$F_2$ $R_{\text{QCD}}$	$\Delta F_2$ $R_{\text{QCD}}$	$xF_3$ ( $R=0.1$ )	$xF_3$ $R_{\text{QCD}}$	$\Delta xF_3$ $R_{\text{QCD}}$	$x$	$Q^2$	$F_2$ ( $R=0.1$ )	$F_2$ $R_{\text{QCD}}$	$\Delta F_2$ $R_{\text{QCD}}$	$xF_3$ ( $R=0.1$ )	$xF_3$ $R_{\text{QCD}}$	$\Delta xF_3$ $R_{\text{QCD}}$
0.015	1.26	1.256	1.287	0.051	0.171	0.165	0.058	0.550	12.59	0.241	0.241	0.017	0.217	0.218	0.071
	2.00	1.308	1.343	0.058	0.376	0.366	0.056		19.95	0.232	0.231	0.015	0.167	0.168	0.044
	3.16	1.499	1.537	0.084	0.309	0.303	0.076		31.62	0.209	0.206	0.014	0.207	0.209	0.029
	5.01	1.370	1.402	0.116	0.434	0.431	0.106		50.12	0.202	0.198	0.018	0.170	0.171	0.033
	7.94	1.548	1.584	0.269	-	-	-		79.43	0.203	0.199	0.020	0.167	0.169	0.031
									125.89	0.156	0.150	0.019	0.169	0.170	0.024
									199.53	0.128	0.120	0.040	0.130	0.130	0.044
0.045	1.26	1.134	1.134	0.050	0.448	0.440	0.143	0.650	12.59	0.150	0.150	0.018	0.161	0.163	0.080
	2.00	1.350	1.359	0.047	0.627	0.620	0.089		19.95	0.121	0.120	0.010	0.170	0.171	0.033
	3.16	1.348	1.363	0.044	0.615	0.608	0.062		31.62	0.139	0.138	0.015	0.121	0.122	0.039
	5.01	1.528	1.545	0.059	0.513	0.508	0.072		50.12	0.112	0.111	0.015	0.071	0.072	0.030
	7.94	1.647	1.662	0.081	0.696	0.693	0.094		79.43	0.100	0.098	0.016	0.058	0.058	0.028
	12.59	1.520	1.531	0.113	0.647	0.646	0.116		125.89	0.095	0.092	0.014	0.098	0.099	0.018
	19.95	1.068	1.071	0.197	0.630	0.631	0.182		199.53	0.071	0.068	0.020	0.076	0.076	0.023
0.080	1.26	1.247	1.244	0.128	-	-	-								
	2.00	1.447	1.445	0.055	0.620	0.615	0.182								
	3.16	1.486	1.487	0.046	0.774	0.769	0.103								
	5.01	1.460	1.464	0.044	0.668	0.666	0.070								
	7.94	1.542	1.545	0.051	0.657	0.655	0.069								
	12.59	1.592	1.591	0.068	0.781	0.781	0.085								
	19.95	1.584	1.576	0.090	0.771	0.771	0.098								
	31.62	1.241	1.228	0.166	0.662	0.662	0.162								
0.150	2.00	1.194	1.183	0.109	-	-	-								
	3.16	1.186	1.180	0.036	0.733	0.732	0.135								
	5.01	1.284	1.280	0.028	0.689	0.689	0.073								
	7.94	1.241	1.235	0.025	0.878	0.878	0.046								
	12.59	1.242	1.232	0.028	0.854	0.855	0.042								
	19.95	1.305	1.292	0.036	0.789	0.790	0.049								
	31.62	1.290	1.270	0.046	0.846	0.847	0.055								
	50.12	1.188	1.161	0.075	0.799	0.799	0.080								
	79.43	0.917	0.889	0.251	0.705	0.704	0.239								
0.250	3.16	1.874	1.868	0.724	-	-	-								
	5.01	1.028	1.026	0.039	0.622	0.623	0.161								
	7.94	0.989	0.985	0.026	0.792	0.794	0.076								
	12.59	0.941	0.933	0.024	0.794	0.797	0.048								
	19.95	0.936	0.923	0.026	0.766	0.770	0.042								
	31.62	0.968	0.952	0.033	0.795	0.799	0.050								
	50.12	0.862	0.840	0.034	0.745	0.747	0.042								
	79.43	0.777	0.747	0.053	0.649	0.650	0.057								
	125.89	0.598	0.568	0.279	-	-	-								
0.350	5.01	0.882	0.882	0.189	-	-	-								
	7.94	0.677	0.676	0.027	0.581	0.584	0.108								
	12.59	0.652	0.649	0.023	0.550	0.553	0.060								
	19.95	0.645	0.638	0.024	0.466	0.469	0.047								
	31.62	0.637	0.627	0.027	0.509	0.512	0.048								
	50.12	0.600	0.587	0.028	0.559	0.563	0.041								
	79.43	0.619	0.597	0.037	0.499	0.500	0.045								
	125.89	0.719	0.684	0.076	0.266	0.266	0.083								
0.450	7.94	0.498	0.498	0.041	-	-	-								
	12.59	0.421	0.419	0.020	0.450	0.452	0.068								
	19.95	0.398	0.395	0.019	0.304	0.306	0.043								
	31.62	0.388	0.382	0.020	0.317	0.319	0.038								
	50.12	0.354	0.347	0.021	0.337	0.340	0.036								
	79.43	0.385	0.375	0.026	0.315	0.317	0.037								
	125.89	0.292	0.279	0.028	0.303	0.303	0.032								
	199.53	0.307	0.290	0.132	0.300	0.302	0.139								

sured in muon scattering by the EMC group [16] shows a level difference of about 10%, possibly due to systematic normalization differences among experiments. The  $x$ -dependence of the two structure functions is very similar. This comparison indicates agreement with the mean squared quark charge prediction at the 10% level.

(2) Measurement of the GLS sum rule gives

$$\int_0^1 F_3 dx = 2.83 \pm 0.20$$

consistent with the Quark-Parton model and QCD with  $\Lambda < 525$  MeV.

(3) Fits to  $F_2$  in leading order and second order give, with statistical errors,

$$A_{\text{LO}}^{F_2} = 360 \pm 100 \text{ MeV}$$

$$A_{\text{MS}}^{F_2} = 340 \pm 110 \text{ MeV}$$

for a particular choice of gluon distribution. Variations of the parameters in the gluon distribution over reasonable limits indicate an additional rms uncertainty of approximately 50 MeV. Other systematic uncertainties, such as  $R$  and flux uncertainties, indicate a net systematic error comparable to the statistical error.

(4) A fit to  $xF_3$  in leading order gives, with statistical error,

$$A_{\text{LO}}^{xF_3} = 88 \begin{matrix} +163 \\ -78 \end{matrix} \text{ MeV.}$$

A fit assuming  $R=0$  and  $\bar{q}=0$  for  $x>0.4$ , so that the better determined  $F_2$  may be used at large  $x$ , gives

$$A_{\text{LO}}^{xF_3/F_2} = 266 \begin{matrix} +114 \\ -104 \end{matrix} \text{ MeV.}$$

The systematic errors (Table 5) are clearly smaller than the statistical errors for the two fits.

(5) Second order fits [22, 23] to  $xF_3$  give somewhat different values of  $A$ , although the values of  $\alpha_S(Q_0^2=12.6 \text{ GeV}^2)$  are not so strikingly different (Table 6).

## References

1. R. Blair et al.: Phys. Rev. Lett. **51**, 343 (1983)
2. D.A. Edwards, F.J. Sciulli: A second generation narrow band beam. Fermilab TM-660 (unpublished)
3. R. Blair et al.: A monitoring and calibration system for neutrino flux measurement in a high energy dichromatic neutrino beam. Nevis preprint (1983), Fermilab-Pub-83/26-Exp. Submitted to Nucl. Instrum. Methods
4. A. Bodek et al.: Z. Phys. C - Particles and Fields **18**, 289 (1983)
5. B.C. Barish et al.: IEEE Trans. Nucl. Sci. **NS-25**, 532 (1978)
6. J. Lee: Measurements of  $\nu_\mu N$  charged current cross sections from  $E_\nu=25 \text{ GeV}$  to  $E_\nu=260 \text{ GeV}$ , Ph.D. Thesis, Caltech, Pasadena, CA (1980)
7. R. Blair: A total cross section and Y distribution measurement for muon type neutrinos and antineutrinos on iron, Ph.D. Thesis, Caltech, Pasadena, CA (1982)
8. H. Abramowicz et al.: Phys. Lett. **107B**, 141 (1981)
9. A. de Rújula, R. Petronzio, A. Savoy-Navarro: Nucl. Phys. **B154**, 394 (1979)
10. CCFRR collaboration: Paper in preparation
11. J.G.H. de Groot et al.: Z. Phys. C - Particles and Fields **1**, 143 (1979)
12. H. Abramowicz et al.: Z. Phys. C - Particles and Fields **17**, 283 (1983)
13. F. Bergsma et al.: Phys. Lett. **123B**, 269 (1983)
14. J.K. Panman: Ph.D. Thesis, University of Amsterdam (1981)
15. S.M. Heagy et al.: Phys. Rev. **D23**, 1045 (1981)
16. J.J. Aubert et al.: Phys. Lett. **105B**, 322 (1981)
17. H.E. Fisk, F. Sciulli: Ann. Rev. Nucl. Part. Sci. **32**, 499 (1982)
18. A.R. Clark et al.: Measurement of the nucleon structure function in iron using 215 and 93 GeV muons. LBL-16286 (1983). Submitted to 1983 Lepton-Photon Conference
19. E. Reya: Phys. Rep. **69**, 195 (1981)
20. G. Altarelli, G. Parisi: Nucl. Phys. **B126**, 298 (1979)
21. H. Georgi, D. Politzer: Phys. Rev. **D14**, 1829 (1976); J. Kaplan, F. Martin: Nucl. Phys. **B115**, 333 (1976)
22. L.F. Abbott, R.M. Barnett: Ann. Phys. **125**, 276 (1980)
23. A. Devoto, D.W. Duke, J.F. Owens, R.G. Roberts: Phys. Rev. **D27**, 508 (1979)
24. G. Altarelli: Phys. Rep. **81**, 1 (1982)
25. D.B. MacFarlane: Nucleon structure from neutrino interactions in an iron target with a study of the singlet quark distribution. Ph.D. Thesis, Caltech, Pasadena, CA (1984)
26. M.V. Purohit: Nucleon structure functions from  $\nu_\mu - Fe$  interactions and a study of the valence quark distribution. Ph.D. Thesis, Caltech, Pasadena, CA (1984)